AAS 07-307

TRAJECTORY AND AEROTHERMODYNAMIC ANALYSIS OF TOWED-BALLUTE AEROCAPTURE USING DIRECT SIMULATION MONTE CARLO

Kristin L. Gates Medlock,* Alina A. Alexeenko,† and James M. Longuski‡

We investigate trajectories and aerothermodynamics of ballute-assisted, low- to high-mass, Mars-entry systems. Ballutes permit aerocapture at higher altitudes and allow for lower thermal protection system (TPS) mass, due to lower heat fluxes, than traditional aeroshells. Because the velocity change is achieved at high altitudes, rarefaction can be considerable. To account for rarefaction we employ the Direct Simulation Monte Carlo (DSMC) method, which is based on kinetic flow modeling. Trajectory calculations are presented for Mars entry with varying vehicle masses (0.1–100 tons). In addition, detailed aerothermodynamic analysis is conducted for the maximum heat flux conditions, for the 0.1 ton case. The DSMC results indicate that the C_D for Mars is higher than the C_D calculated for air at the same Knudsen number. Also, the DSMC analysis predicts a lower heat flux than analytic approximations suggest. Heat flux on the ballute, according to the DSMC analysis, is low enough that a smaller ballute may be used.

INTRODUCTION

BALLUTE aerocapture combines the benefit of capture in a single pass with the advantages of high altitude capture, such as lower heating rates and lower deceleration forces, than achieved with traditional aeroshells. As its name suggests, a ballute is a cross between a balloon and a parachute. The ballute's large area-to-mass ratio facilitates capture at high altitudes. During ballute aerocapture, the orbiter approaches the planetary body on a hyperbolic trajectory, deploying the ballute before entering the atmosphere, as shown in Figure 1. Inside the atmosphere, the vehicle begins to decelerate at a rapidly increasing rate. Once the desired velocity change is achieved, the ballute is released allowing the orbiter to exit the atmosphere, where it can propulsively raise periapsis and achieve the desired orbit.

Research has been conducted to investigate the benefits and feasibility of ballute aerocapture at multiple destinations.[1–14] For this paper, we use the Hypersonic Planetary Aero-assist Simulation System (HyperPASS)[15] to obtain ballute entry trajectories. Aerothermodynamic analysis is performed for specific

* Doctoral Candidate, Purdue University, School of Aeronautics & Astronautics, West Lafayette, Indiana, 701 West Stadium Ave., 47907-2045, Student Member AIAA.
† Assistant Professor, Purdue University, School of Aeronautics & Astronautics, West Lafayette, Indiana, 701 West Stadium Ave., 47907-2045, Member AIAA.
‡ Professor, Purdue University, School of Aeronautics & Astronautics, West Lafayette, Indiana, 701 West Stadium Ave., 47907-2045, Member AAS, Associate Fellow AIAA.

points (e.g. at maximum heat flux) along the trajectories using the DSMC[16] solver SMILE (Statistical Modeling In Low-density Environment).[17]

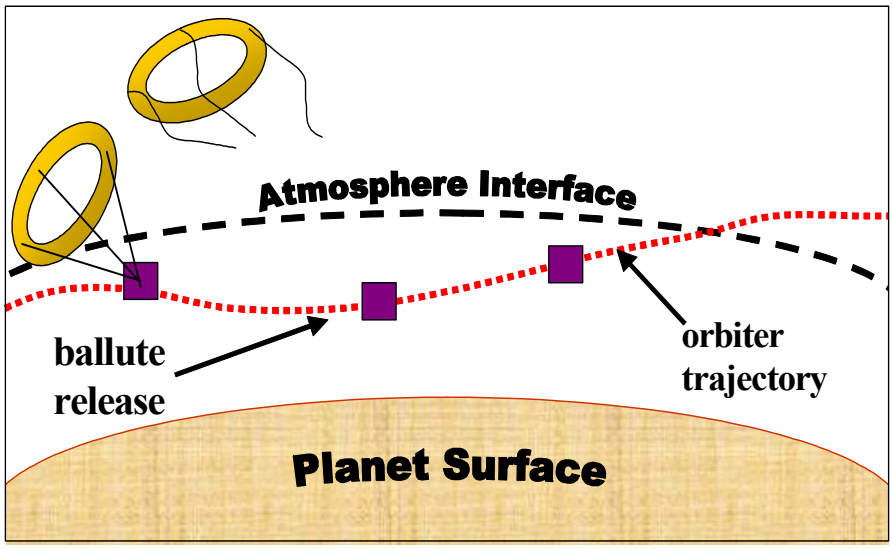

Figure 1 Ballute Aerocapture

BALLUTE VEHICLE SPECIFICATIONS

Previous studies of ballute aerothermodynamics using the DSMC method were conducted for Earth returns and Titan missions by Moss et al.[18] and Gnoffo et al.[19] Moss finds that a 4:1 configuration (ring radius : cross-sectional tube radius, depicted in Figure 2) allows the spacecraft's wake to pass through the torus' ring without disturbing the flow around the ballute. Because of this favorable result, we use the 4:1 ratio for the ballute configurations. [§]

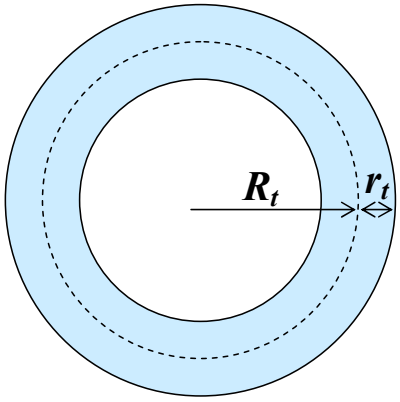

Figure 2 Cross-Sectional View of Tube of Toroidal Ballute

$$r_t = R_t/4 \tag{1}$$

[§] See the notation section, located after the conclusion and acknowledgements, for mathematical nomenclature.

Following this assumption, the ballute cross-sectional area, A, and the ballute surface area, S, are

$$A = \pi R_t^2 \ , \ S = \pi^2 R_t^2 \tag{2}$$

We determine the size of the toroidal ballute by substituting Eq. (2) into the expression for ballistic coefficient:

$$C_B = \frac{m_{s/c} + m_{ball}}{C_D A} = \frac{m_{s/c} + \sigma S}{C_D A} \tag{3}$$

We assume an initial ballistic coefficient of 0.5 and an initial C_D of 2 for each case, allowing us to solve Eq. (3) for the large ballute radius, R_t. Figure 3 and Table 1 display the resulting ballute and spacecraft configurations for each case.

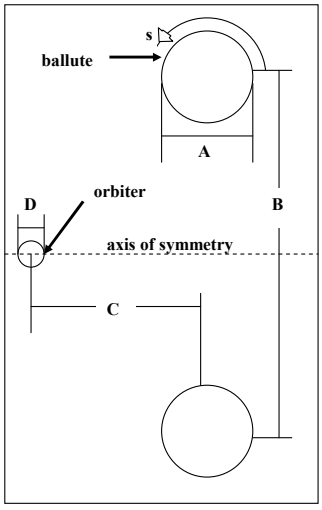

Figure 3 Configuration of the Ballute and Orbiter

Table 1
BALLUTE CONFIGURATIONS

Parameter	0.1 ton case	1 ton case	10 ton case	100 ton case
A	2.866 m	9.063 m	28.66 m	90.63 m
B	11.46 m	36.25 m	114.6 m	262.5 m
C	6.614 m	20.92 m	66.14 m	209.2 m
D	1.600 m	3.438 m	7.406 m	15.96 m

BALLUTE AEROCAPTURE TRAJECTORIES

We perform ballute-aerocapture trajectory simulations using the HyperPASS program, which assumes point-mass vehicle representation, inverse-square gravity field, spherical planetary bodies, rotating atmosphere (with planet), and exponentially interpolated atmosphere. Table 2 gives the vehicle parameters used for the simulations.

Table 2
VEHICLE PARAMETERS FOR BALLUTE SIMULATIONS AT MARS

Parameter	0.1 ton case		1 ton case		10 ton case		100 ton case	
	Orbiter	Ballute	Orbiter	Ballute	Orbiter	Ballute	Orbiter	Ballute
***m*, [kg]**	100	3.223	1000	32.23	10,000	322.3	100,000	3223
***A*, [m^2]**	2.00	1.032×10^2	9.28	1.032×10^3	43.1	1.032×10^4	200	1.032×10^5
***R$_n$*, [m]**	0.798	1.433	1.719	4.532	3.703	14.33	7.979	45.32

The trajectories are propagated using a C_D that varies with Knudsen number. Previous studies of ballute-assisted aerocapture were based on a constant $C_D = 1.37$.[4,13] Knudsen number is defined as the molecular mean-free path divided by the characteristic length:

$$Kn = \frac{\lambda}{L} \tag{4}$$

The mean-free path is inversely proportional to the number density of gas molecules and, therefore, decreases with increasing altitude. The characteristic length of the flow around the towed toroidal ballute is the diameter of the torus tube ($L = 2r_t$). The C_D vs. Kn model that we use is based on Moss' Direct Simulation Monte Carlo (DSMC) results for air[18], depicted in Figure 4. The simulations are initiated at an altitude of 350 km, instead of the typical 150 km Mars entry altitude, so that an initial C_D of 2 can be assumed for all four ballute sizes.

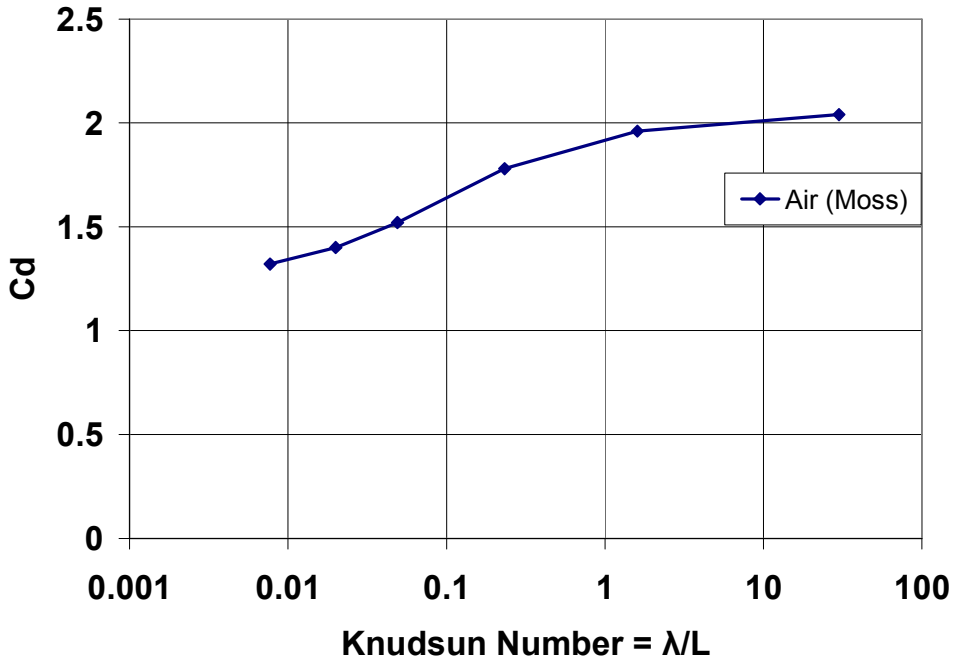

Figure 4 Drag Coefficient as a Function of Knudsen Number for Air[18]

The simulation parameters at Mars are shown in Table 2, with the target apoapsis chosen to achieve a 4-day parking orbit. For all cases presented here, we assume that the ballute is not released.

Table 2
ENTRY AND TARGET CONDITIONS FOR BALLUTE SIMULATION AT MARS

Condition	Mars
Entry/Exit Altitude, km	350
Inertial Entry Speed, km/s	5.877
Inertial Entry FPA, deg	-17.56 to -17.59
Target Apoapsis Altitude, km	97508.2

For the 0.1 ton case, we compare the trajectory calculation with the variable C_D model to the trajectory calculation for a constant C_D model with the same initial conditions. Figure 5 shows the altitude vs. time for 0.1 ton Mars aerocapture with constant and variable C_D. The influence of variable C_D is negligible for the initial part of the trajectory down to an altitude of about 150 km, where the atmosphere is still free molecular. The effects of variable C_D is pronounced at lower altitudes and result in a longer time to exit.

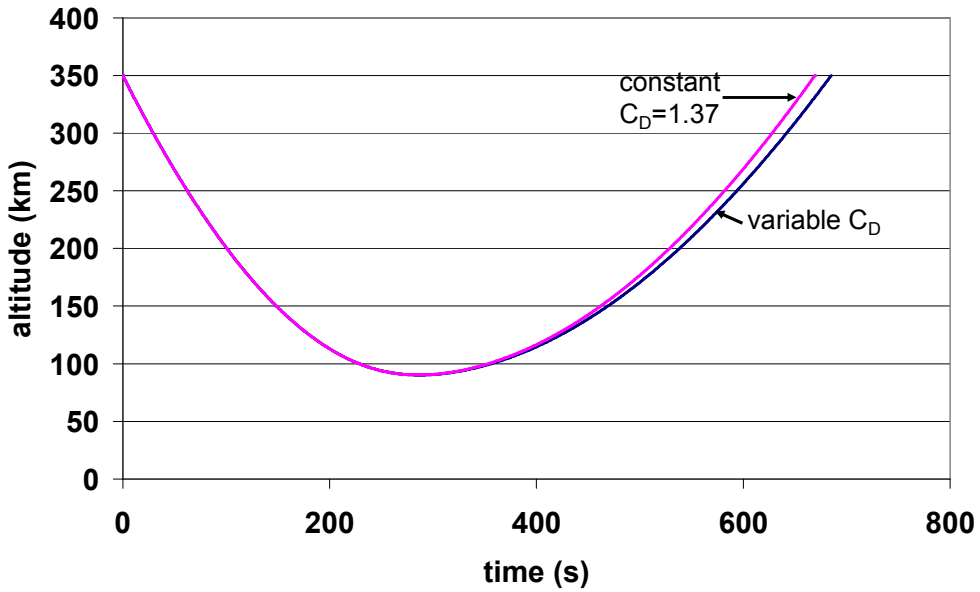

Figure 5 Altitude vs. Time Comparison of Constant CD and Variable CD models for 0.1 ton Case

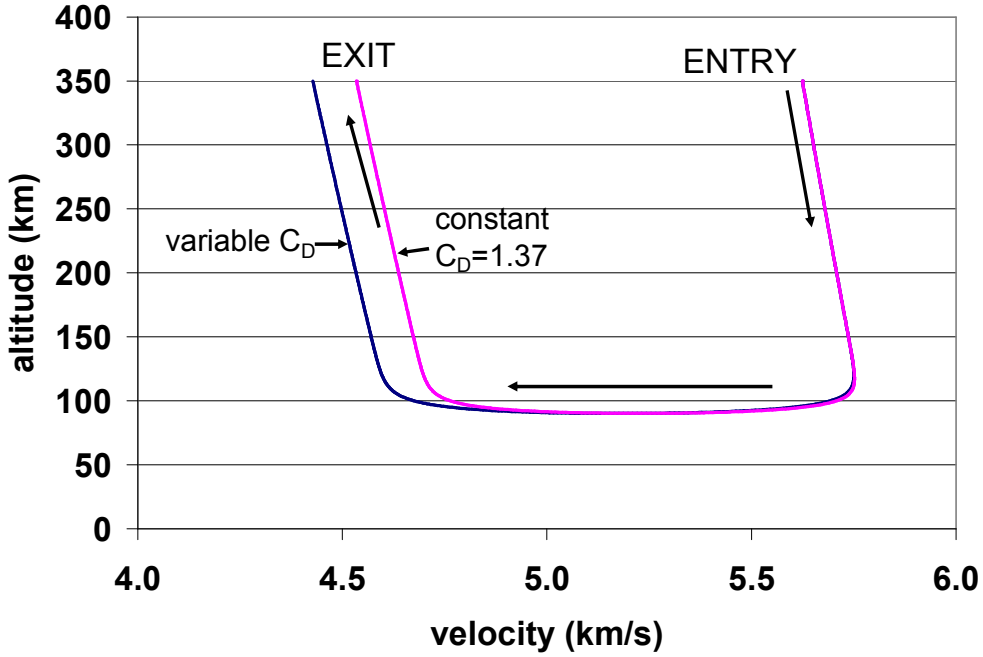

Figure 6 Altitude vs. Velocity Comparison of Constant CD and Variable CD models for 0.1 ton Case

The velocity-altitude map for the constant (1.37) and variable C_D models of 0.1 ton Mars ballute aerocapture is shown in Figure 6. There is a significant difference in exit velocity, 4.43 km/s vs. 4.53 km/s, for a constant C_D and a variable C_D, respectively. Thus, the effects of variable C_D are significant for targeted ballute aerocapture. Note that this comparison is based on the same entry conditions for each model, whereas if the same exit conditions were targeted, then the constant C_D model would predict a trajectory that penetrates deeper into the atmosphere where heating rates are higher.

The stagnation-point heating rates and free-molecular heating rates are calculated by HyperPASS using

$$Q_{stag} = Cv^3\sqrt{\frac{\rho}{R_n}} \tag{5}$$

and

$$Q_{fm} = \frac{1}{2}\rho v^3 \tag{6}$$

Equation (5) is similar to the Sutton-Graves stagnation-point heating approximation[20].

The predicted stagnation point heating rates for the constant and variable C_D models are shown in Figure 7. The constant C_D model with the same entry conditions predicts a trajectory with a maximum heating rate 2% higher than the more accurate variable C_D model. If the trajectories were calculated for the same target orbit and different entry-flight-path angle, the heating rate for constant C_D would be even higher.

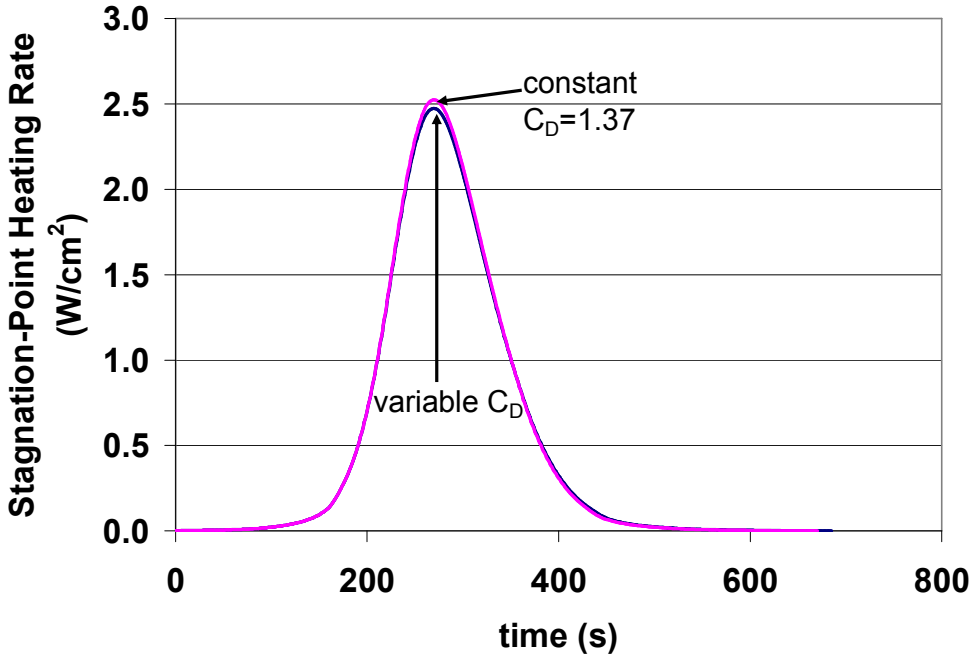

Figure7 Heating Rate vs. Time Comparison of Constant CD and Variable CD models for 0.1 ton Case

Now, we present results comparing four different sized ballute systems using the variable C_D model. Figures 8 and 9 show the altitude and velocity trajectory results for the four cases. Because the initial ballistic coefficient, $C_B = m/(C_D A)$, is the same for each case, the altitude and velocity profiles are nearly identical for all four cases. The maximum difference in the time to reach the exit altitude is about 3 seconds.

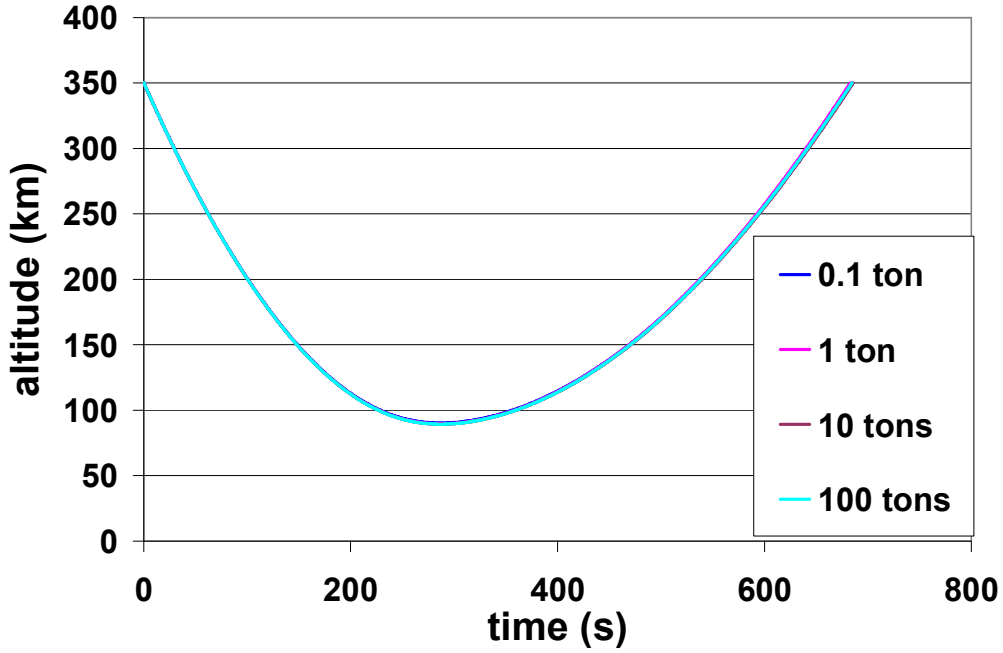

Figure 8 Altitude vs. Time Since Entry for Mars Ballute Aerocapture Trajectories

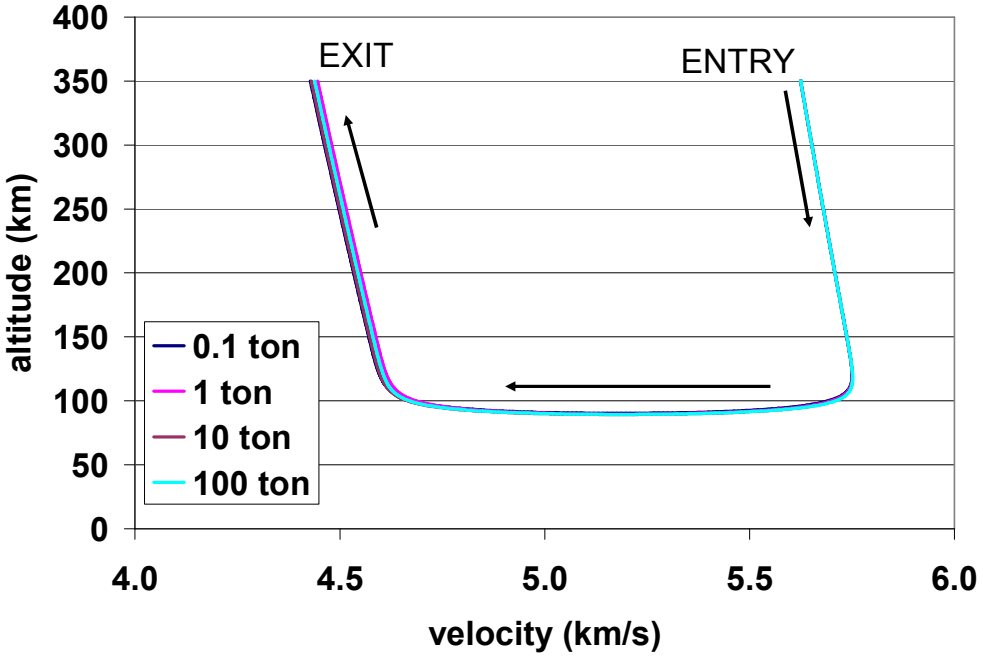

Figure 9 Altitude-Velocity for Mars Ballute Aerocapture Trajectories

Figure 10 shows altitude versus Knudsen number. Knudsen number changes almost exponentially with altitude, due to the exponential change in atmospheric density. For all cases, altitudes above 250 km are in the free-molecular flow regime. The simulations indicate that peak conditions (such as heating, pressure, and deceleration force) occur just prior to periapsis (the lowest point in the trajectory). One can see that, depending on the case, the flow around the ballute is characterized by entirely different flow phenomena near periapsis. The smallest case (0.1 ton) is in the rarefied regime near periapsis. However, the larger 100 ton case is shifted and its lowest point is clearly in the continuum regime. Both the 1 ton case and the 10 ton case are in the slip flow regime which is characterized by 0.001 Kn < 0.05. Accurate modeling of aerothermodynamics near periapsis will require entirely different approaches, for the different flow regimes.

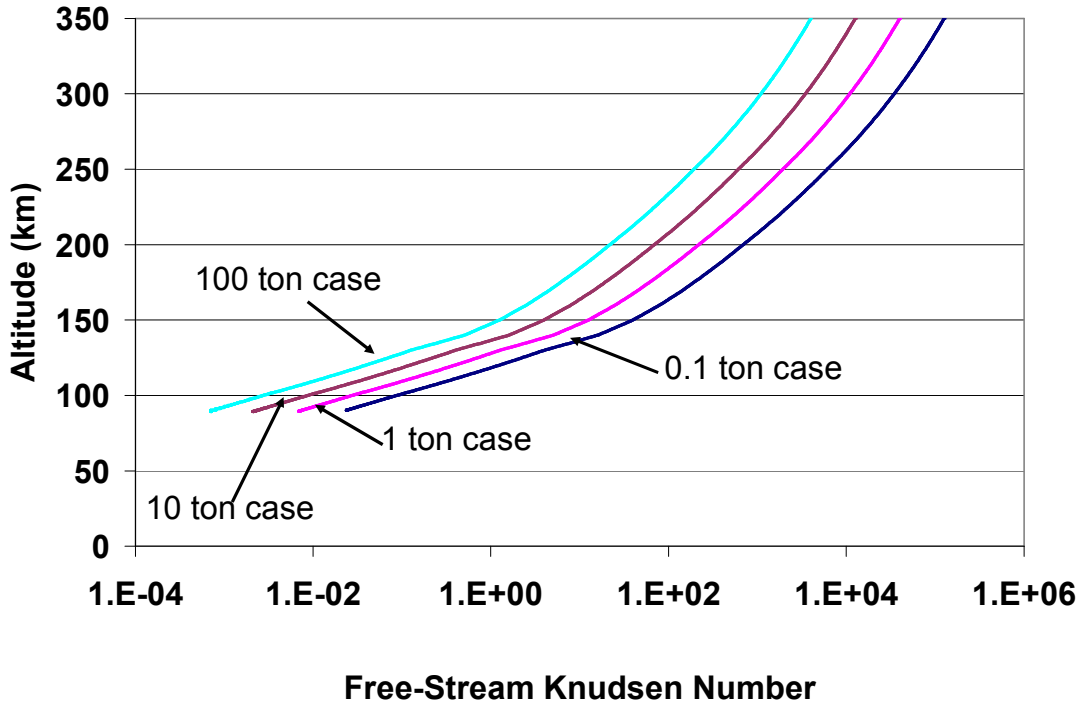

Figure 10 Altitude vs. Knudsen Number for Mars Ballute Aerocapture Trajectories

Figure 11 displays the stagnation point heating rates for each trajectory as a function of time and Figure 12 shows the stagnation-point heating rate as a function of Knudsen number. Because the stagnation-point heating rate is inversely proportional to the square root of the nose radius (or the ballute's tube radius), the larger ballutes have lower heating rates throughout the trajectory. One candidate ballute material is Kapton, which has a heating limit around 5 W/cm^2.[1] The results in Figure 11 indicate that smaller ballutes may be feasible for the heavier cases.

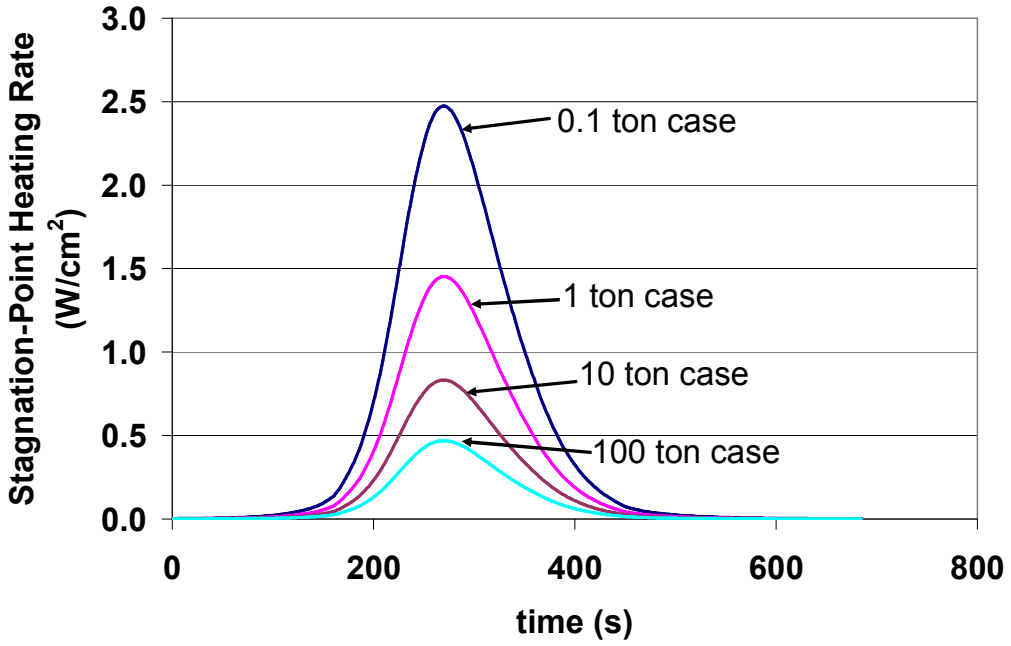

Figure 11 Ballute Stagnation-Point Heating Rate vs. Time Since Entry for Mars Ballute Aerocapture

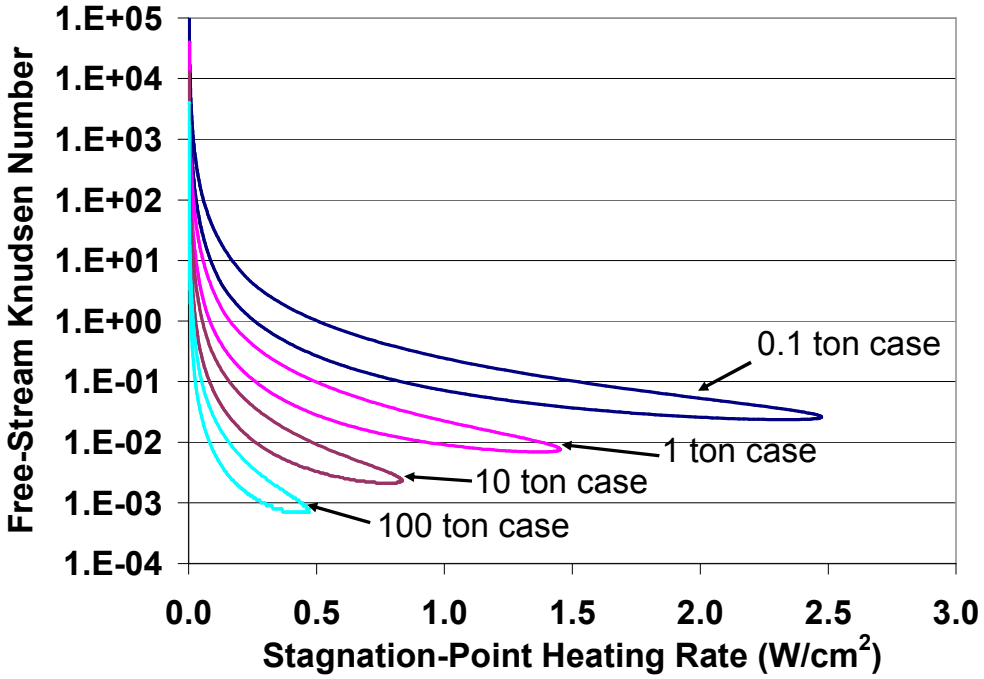

Figure 12 Stagnation Point Heating Rate vs. Knudsen Number for Mars Ballute Aerocapture Trajectories

The variable C_D model used in the trajectory calculations was based on aerothermodynamics simulations for Earth entry. In the rest of the paper, we apply the DSMC modeling to assess the aerothermodynamics of Mars entry for the 0.1 ton case. Table 3 displays the trajectory data, for the 0.1 ton case, at the altitude of maximum heat flux. We apply the DSMC modeling at these conditions.

Table 3
BALLUTE TRAJECTORY AT MAXIMUM HEAT FLUX FOR THE 0.1 TON CASE

time since entry (sec)	269.09	**orbiter stag. point heating (W/cm^2)**	3.3150
atm. density (kg/m^3)	5.2688×10^{-7}	**ballute stag. point heating (W/cm^2)**	2.4736
altitude (km)	90.988	**free molecular heating (W/cm^2)**	4.0987
planet rel. velocity (km/s)	5.3784	**dynamic pressure (N/m^2)**	7.6206
planet rel. FPA (deg)	-1.0170	**total acceleration (g's)**	1.1162
Drag (N)	1130.3	**Knudsen Number**	0.0263

DSMC METHOD

SMILE[17] is a 2D/axisymmetric code that provides both time-accurate unsteady flow and steady-state flow simulations. For the Martian study, we use an eight species (CO_2, N_2, CO, O_2, O, N, NO, and C) gas model with 50 dissociation and recombination chemical reactions[21] and exchange between translational, rotational, and vibrational modes. We use the variable-hard-sphere molecular model and the Larsen-Borgnakke[22] model for energy exchange between kinetic and internal modes. We use a free-stream atmosphere composition of 96 % CO_2 and 4% N_2 for Mars. A noncatalytic model surface, with a constant wall temperature of 500K, is assumed. The gas-surface interactions are assumed to be diffuse, with full energy accommodation.

Since HyperPASS assumes that the atmosphere rotates with the planetary body, the planet relative velocity is used as the free-stream velocity (V_∞) in the DSMC analysis. The flight path angle is very small and is assumed to be equivalent to 0 degrees; this assumption allows us to use the axisymmetric flow model. Lastly, we assume a steady state flow since the hypersonic flow characteristic time scale is on the order of 10^{-6} sec which is much smaller than the time scale of vehicle altitude variation (seconds).

FLOW CONDITIONS

Before running SMILE, several simulation parameters must be estimated, including cell size, Knudsen number, and simulation time. For DSMC, the cell dimension, Δx must be less than the mean free path, λ. In order to calculate λ (and other values given in Table 4), we use the Gas Dynamics Toolbox provided by Alexeenko[23] to calculate mixture viscosity and mean-free path for variable-hard-sphere (VHS) models for mixtures at the given altitude. The temperature and density values are from the Mars COSPAR-90 atmosphere model. [24] For all cases, the specific heat ratio is 1.4, the viscosity is 6.75×10^{-6}, and the free-stream temperature is 139 K.

Table 4
FLOW CONDITIONS

Case	atm. density (kg/m^3)	atm. pressure (N/m^2)	free-stream velocity (km/s)	mean-free path (m)	ballute char. length (m)	ballute *Kn*	ballute *Re*
0.1 ton	5.27×10^{-7}	1.40×10^{-2}	5.378	7.33×10^{-2}	2.86	2.56×10^{-2}	1.11×10^{3}
1 ton	5.74×10^{-7}	1.53×10^{-2}	5.379	6.24×10^{-2}	9.06	6.90×10^{-3}	4.15×10^{3}
10 ton	5.88×10^{-7}	1.57×10^{-2}	5.391	6.09×10^{-2}	28.66	2.10×10^{-3}	1.35×10^{4}
100 ton	5.880×10^{-7}	1.57×10^{-2}	5.393	6.09×10^{-2}	90.63	6.72×10^{-4}	4.26×10^{4}

The Knudsen and Reynolds numbers are the governing nondimensional parameters that determine the flow regime for the ballute. The Reynolds number characterizes the relative importance of inertial and viscous forces. For large Reynolds numbers, the flow transitions from laminar, viscous flow to turbulent flow. Knudsen number characterizes the importance of flow rarefaction and non-equilibrium. For continuum flows ($Kn < 10^{-3}$), molecular-mean-free path is negligible compared to characteristic length scale and the aerodynamic modeling can be based on continuum conservation laws, such as the Navier-Stokes equations. As the mean-free path increases, the continuum hypothesis for description of the gas as a continuum medium breaks down and the modeling needs to be based on the kinetic theory of gases. At very large Knudsen numbers ($Kn > 50$), the mean-free path of molecules is much larger than the problem size and the effect of intermolecular collisions is negligible. Such collisionless flows are called free-molecular. The DSMC method is currently the most powerful approach for simulation of hypersonic, rarefied gas flows and, therefore, it is applied here for calculation of aerothermodynamic parameters in the 0.1 ton ballute aerocapture case.

Table 4 shows that the 0.1 ton case is in rarefied, laminar flow and we will use DSMC for aerothermodynamic analysis. The 10 ton and 100 ton cases are in near-continuum and slip flow regimes and the Navier-Stokes equations can be used. The aerothermodynamic simulations based on Navier-Stokes equations can also be used to analyze the 1 ton case because the Kn is low enough.

For this problem, there are different characteristic lengths associated with the vehicle, the ballute, and the tethers. It is therefore necessary to calculate different Knudsen numbers for each of the various characteristic lengths. For the 0.1 ton case, the Knudsen numbers corresponding to the spacecraft ($Kn = 4.58\text{x}10^{-2}$, assuming a characteristic length of 1.60 m) and ballute ($Kn = 2.56\text{x}10^{-2}$, assuming a characteristic length of 2.86 m) indicate that they are in the rarefied flow regime, while the tethers ($Kn =$ 7.32, assuming a characteristic length of 0.01 m) will approach a free-molecular flow regime as the diameter of the tether approaches zero.

There are two requirements when determining the time step, Δt, used in the DSMC simulation. First, Δt must be less than the mean collision time (or, in other words, the mean distance traveled in Δt must be less than the mean-free path). Mean collision time, τ, is given by:

$$\tau = \frac{\lambda}{\overline{v'}} \tag{7}$$

where the average thermal velocity for each species is found using Maxwell's equilibrium distribution.

$$\overline{v'_i} = \sqrt{\frac{8}{\pi} RT} \tag{8}$$

Once the average thermal velocity has been calculated for each molecular species [using Eq. (8)], the average thermal velocity for the mixture can be determined.

$$\overline{v'} = .96\ \overline{v'_{CO_2}} \ + \ .04\ \overline{v'_{N_2}} \tag{9}$$

Equation (9) gives an average thermal velocity of 462.94 m/s for the Martian atmosphere, where $\overline{v'_{CO_2}}$ and $\overline{v'_{N_2}}$ are calculated using Eq. (8). Finally, using Eq. (7), we calculate the mean collision time, τ, to be 0.17 milliseconds for the 0.1 ton case.

The second constraint on Δt states that a molecule must cross no more than one cell in Δt, which means that Δt must be less than the residence time where,

$$\tau_{res} \approx \frac{\Delta x}{V_\infty} \tag{10}$$

Using Eq. (10), and assuming a Δx of 0.04 m for the 0.1 ton case, we calculate that τ_{res} is 7.44 microseconds. The residence time is smaller than the mean collision time and, therefore, the selected time step must be less than the residence time.

An estimation of the simulation time until a steady state is reached is made by doubling the time it takes a molecule to pass from one side of the simulated flowfield to the other. To determine this time, we will again use Maxwell's equilibrium distribution, Eqn. (7), to calculate the average thermal velocities for both the carbon dioxide and nitrogen molecules. The slower of the average thermal velocities is carbon dioxide (at 458.29 m/s), so the time it takes a carbon dioxide molecule to move across the flowfield two times will be used as an estimation for the required simulation time. The simulation flow field is 22 m long and using the thermal velocity of CO_2, the estimated a simulation time until steady state is 0.096 seconds.

Based on this criteria, the total number of cells used in the DSMC calculations was 220 thousand with a total of about 1.2 million molecules.

DSMC RESULTS

Figure 13 shows a contour plot of flowfield Mach number, with a hypersonic free-stream flow (red region) of about Mach 28. The flowfield is complex hypersonic flow characterized by the interaction of the spacecraft and ballute shock waves (the shock is depicted by yellow and green contours). Subsonic complex wake can be seen behind both the spacecraft and the ballute.

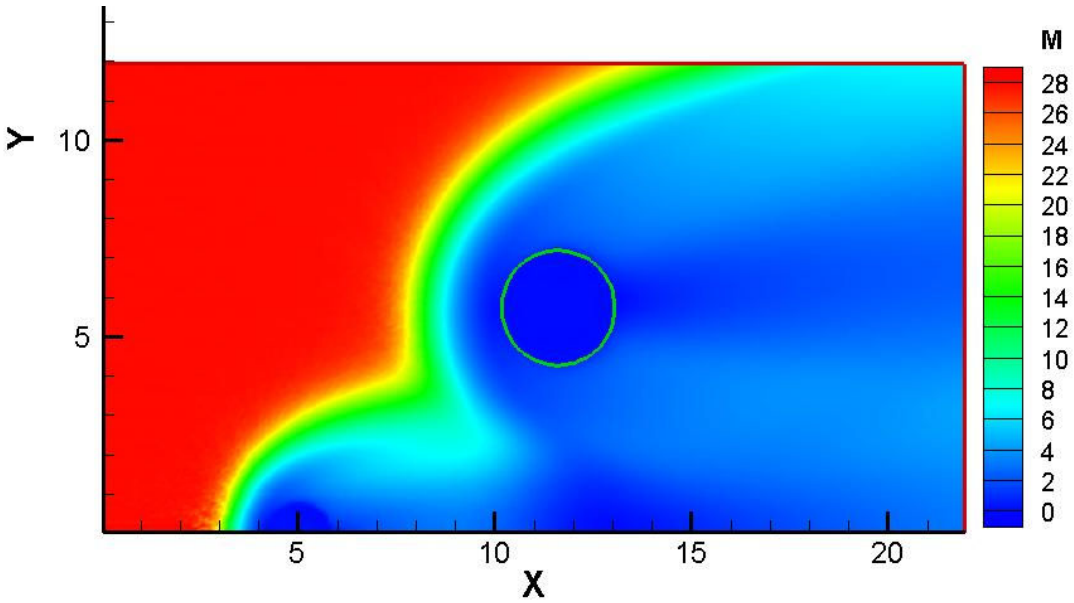

Figure 13 Flowfield Mach Number from DSMC Analysis

Figure 14 shows the flowfield pressure, with a free-stream pressure (blue region) of 0.014 Pa. It is seen that the maximum pressure is on the ballute's surface. DSMC also calculates the surface pressure on the ballute and spacecraft (displayed in Figure 15).

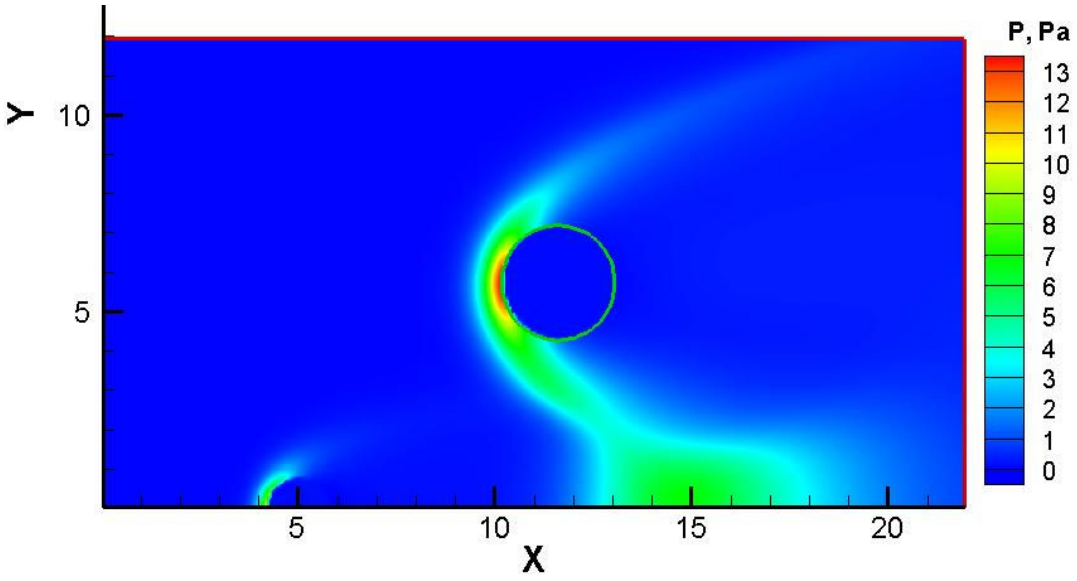

Figure 14 Flowfield Pressure from DSMC Analysis

Based on the pressure distributions and the skin friction distributions, we can calculate the aerodynamic drag forces and, in turn, compute the C_D. The C_D is found by first integrating the pressure and in-plane shear stress, over the surfaces of the spacecraft and ballute, to find the total drag force, D. Because we have an axially symmetric body at zero angle of attack, the lifting force is zero and therefore the total force on the ballute is equal to the drag force.

$$C_D = \frac{D}{\frac{1}{2}\rho_\infty V_\infty^2 A} \tag{11}$$

The drag force can then be used in Eq. (11) to calculate the C_D. We find that the combined drag force on the ballute and spacecraft is 1187.7 N. Based on Moss' calculation for air, the C_D was assumed to be 1.32, which is close to the constant value of 1.37 typically assumed for toroidal ballutes. Our calculation using DSMC gives a C_D of 1.48. So, the DSMC predicted C_D for Mars is higher than the C_D calculated for air at the same Knudsen number

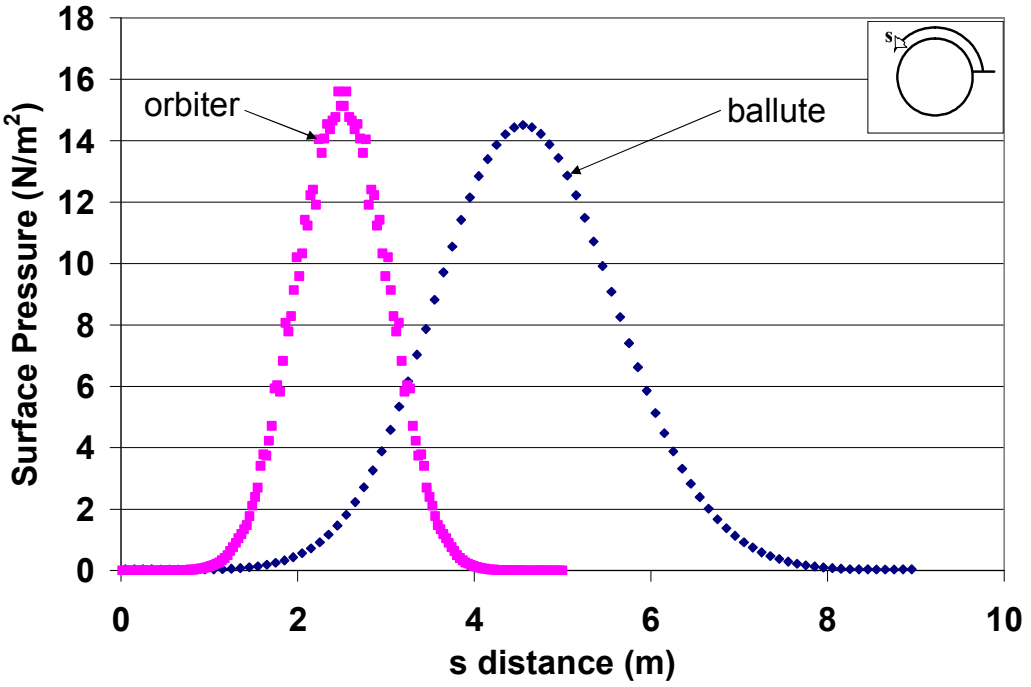

Figure 15 Pressure Distribution on the Surface of the Ballute and Spacecraft

Figure 16 shows a plot of the flowfield temperature with a free-stream temperature of 139 K (dark blue region). For high Mach number (or high hypersonic) flow, the temperature increases dramatically in the shock region. High temperature flow will have to be considered for analyzing the heat flux on the ballute and spacecraft. High temperatures lead to CO_2 dissociation in the atmosphere, causing a lot of chemical reactions. The chemical reactions produce radicals such as atomic oxygen that could potentially react with the ballute material, which will have an effect on the type of ballute material chosen.

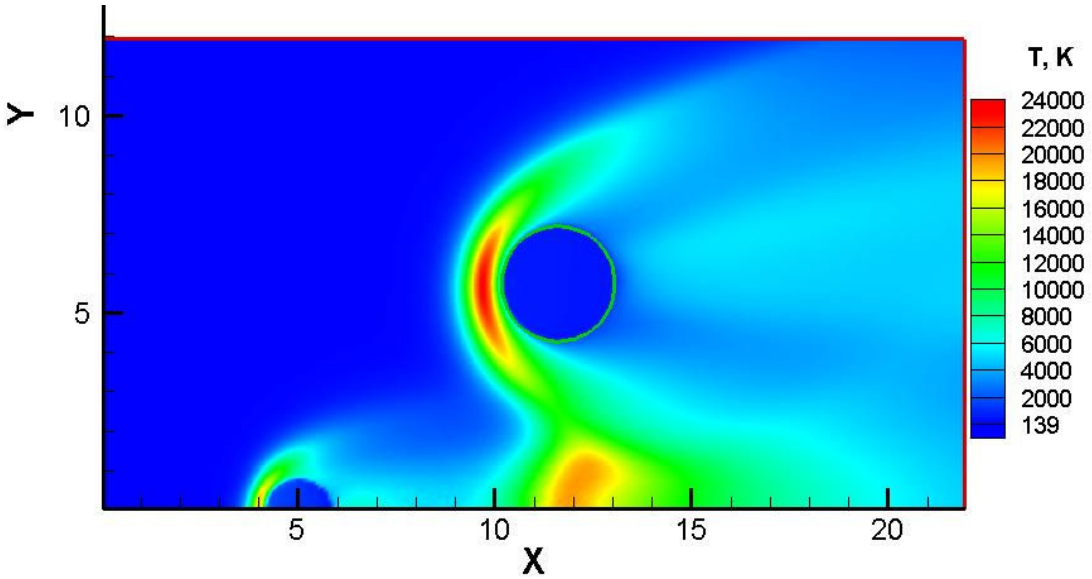

Figure 16 Flowfield Temperature from DSMC Analysis

Figure 17 is a plot of the heat flux along the surface of the ballute and spacecraft. The maximum heating points on each surface are the stagnation points of the spacecraft and the ballute. Equation (5) predicts a stagnation-point heating rate of 2.47 W/cm^2 on the ballute, but the DSMC calculation resulted in a much lower heating rate of 1.63 W/cm^2 (34% lower). Assuming the ballute is made of Kapton, with a maximum heating tolerance of 4-5 W/cm^2, the lower heating rate from the DSMC simulation indicates that an even smaller ballute may be feasible. Using the stagnation-point heating rate of 1.63 W/cm^2 in Eq. (5) results in a stagnation-point heating coefficient, C, of 1.73x10^{-8} kg$^{1/2}$/m (we had assumed a C of 2.62x10^{-8} kg$^{1/2}$/m, based on the Sutton-Graves model). The DSMC predicted stagnation-point heating rate on the orbiter is 3.09, which is only about 6 % smaller than the 3.31 W/cm^2 heating rate predicted by HyperPASS (using the Sutton-Graves approximation). Also, the stagnation-point heating rate on the orbiter is higher than on the ballute due to its smaller effective nose radius (see Table 2).

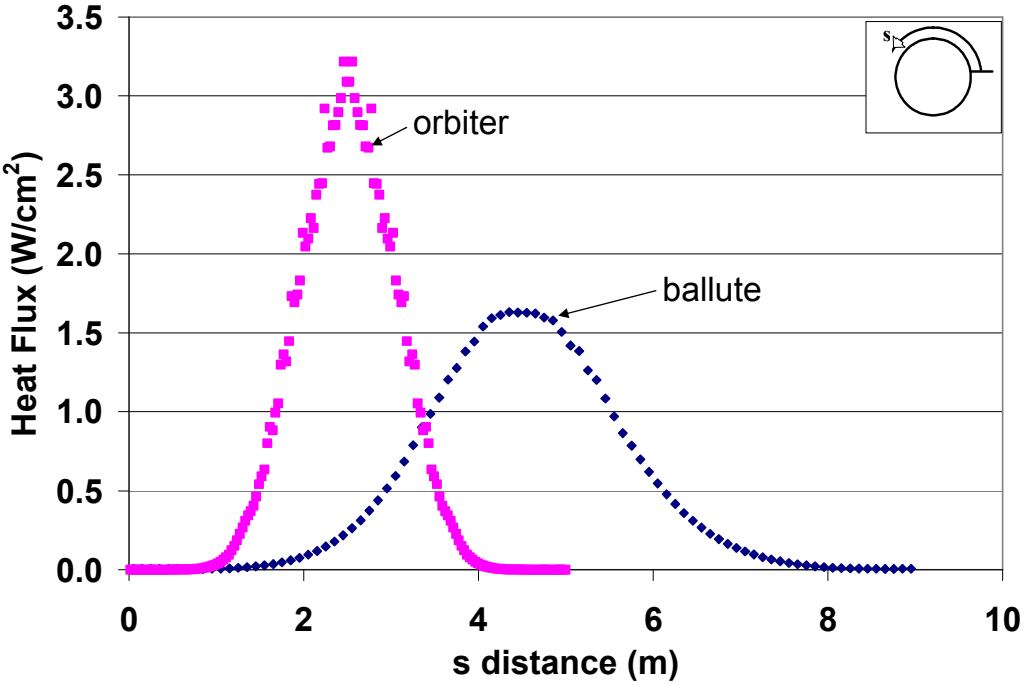

Figure 17 Heat Flux on the Surface of the Ballute and Spacecraft

CONCLUSIONS

We have calculated high-mass ballute-aerocapture trajectories for Mars, in which we vary system mass with the same initial ballistic coefficient. The effects of C_D variation along the trajectory were studied by comparing trajectories with a constant C_D = 1.37 model (used in previous studies) and a variable C_D model (based on recent aerothermodynamics calculations for Earth ballute-assisted entry). Variable C_D affects the exit velocity and the maximum heating rate. Based on the comparison for 0.1 ton case, the difference in exit velocity is 107 m/s. Targeting the same orbit (with a different entry-flight-path angle), based on trajectory simulations with a constant C_D, predicts a deeper descent into the atmosphere and, therefore, higher heating. A comparison of the variable C_D model for Mars atmosphere was carried out by applying the DSMC simulations for the 0.1 ton case at the altitude of maximum heat flux. The DSMC results indicate that the C_D for Mars is higher than the C_D calculated for air at the same Knudsen number by 12%. Also, the DSMC analysis predicts a lower heat flux than estimated by the Sutton-Graves model (about 34% lower). Heat flux on the ballute, according to the DSMC analysis, is low enough that a smaller ballute (larger ballistic coefficient) may be used.

ACKNOWLEDGMENTS

This work is sponsored in part by a NASA Graduate Student Research Program (GSRP) fellowship from Marshall Space Flight Center (MSFC), under contract number NNM05ZA11H. We would like to thank the In-Space Propulsion Team for their support, especially Bonnie F. James (GSRP Technical Advisor) and Michelle M. Munk of MSFC. DSMC simulations were carried out on 16 CPU SunFire server made available through Sun Microsystems, Inc. Academic Excellence Grant, award #T-US-900056-B.

NOTATION

A = cross-sectional area, m^2
C = stagnation point heating coefficient, $kg^{1/2}/m$
C_B = ballistic coefficient, kg/m^2
C_D = drag coefficient
D = drag force, N
g = standard freefall acceleration, 9.80665 m/s^2
K_n = Knudsen Number
L = characteristic length, m
m = mass, kg
Q = heating rate, W/cm^2
R = specific gas constant, J/(kg K)
R_e = Reynold's Number
R_n = nose radius, m
S = surface area, m^2
T = temperature, K
V_∞ = freestream velocity, km/s
v = speed, km/s
v' = thermal velocity, km/s
λ = mean free path, m
ρ = atmospheric density, kg/m^3
σ = areal density of ballute material, kg/m^2
τ = mean collision time, s
τ_{res} = residence time, s

REFERENCES

1. McRonald, A. D., "A Light-Weight Inflatable Hypersonic Drag Device for Planetary Entry," Association Aeronautique de France Conference at Arcachon France, March 16-18, 1999.

2. McRonald, A. D., "A Light-Weight Inflatable Hypersonic Drag Device for Venus Entry," AAS/AIAA Astrodynamics Specialist Conference, Girdwood, Alaska, American Astronautical Society, AAS Paper 99-355, Aug. 16-19, 1999.

3. McRonald, A. D., "A Light-Weight Hypersonic Inflatable Drag Device for a Neptune Orbiter," AAS/AIAA Space Flight Mechanics Meeting, Clearwater, FL, AAS Paper 00-170, Jan. 23-26, 2000.

4. Hall, J. L. and Le, A. K., "Aerocapture Trajectories for Spacecraft with Large, Towed Ballutes," 11th Annual AAS/AIAA Space Flight Mechanics Meeting, Santa Barbara, CA, AAS 01-235, Feb. 11-15, 2001.

5. Gnoffo, P. A. and Anderson, B. P., "Computational Analysis of Towed Ballute Interactions," AIAA 2002-2997, 8th AIAA/ASME Joint Thermophysics and Heat Transfer Conference, St. Louis, MO, June 24-26, 2002.

6. Miller, K. L., Gulick, D., Lewis, J., Trochman, B., Stein, J., Lyons, D. T., and Wilmoth, R., "Trailing Ballute Aerocapture: Concept and Feasibility Assessment," 39th AIAA/ASME/ASEE Joint Propulsion Conference and Exhibit, Huntsville, AL, AIAA Paper 2003-4655, July 20-23, 2003.

7. Westhelle, C. H. and Masciarelli, J. P., "Assessment of Aerocapture Flight at Titan Using a Drag-only Device," 2003 AIAA Atmospheric Flight Mechanics Conference and Exhibit, Austin, TX, AIAA Paper 2003-5389, Aug. 11-14, 2003.

8. Lyons, D. T., and McRonald, A. D., "Entry, Descent and Landing using Ballutes," presentation, 2nd International Planetary Probe Workshop, NASA Ames Research Center, Moffet Field, CA, Aug. 2004.

9. Johnson, W. R., and Lyons, D. T., "Titan Ballute Aerocapture Using a Perturbed TitanGRAM Model," AIAA Atmospheric Flight Mechanics Conference and Exhibit, Providence, RI, AIAA Paper 2004-5280, Aug. 16-19, 2004.

10. Lyons, D. T. and Johnson, W. R., "Ballute Aerocapture Trajectories at Neptune," AIAA Atmospheric Flight Mechanics Conference and Exhibit, Providence, RI, AIAA Paper 2004-5181, Aug. 16-19, 2004.

11. Lyons, D. T. and Johnson, W. R., "Ballute Aerocapture Trajectories at Titan," *Advances in the Astronautical Sciences*, Vol. 116, Supplement, pp. 1–20, 2004.

12. Richardson, E. H., Munk, M. M., James, B. F., Moon, S. A., "Review of NASA In-Space Propulsion Technology Program Inflatable Decelerator Investments," 18th AIAA Aerodynamic Decelerator Systems Technology Conference and Seminar, Munich, Germany, AIAA Paper 2005-1603, May 23–26, 2005.

13. Medlock, K. L. Gates, Longuski, J. M., and Lyons, D. T., "A Dual-Use Ballute for Entry and Descent During Planetary Missions," 3rd International Planetary Probe Workshop, Attica, Greece, June 27 – July 1, 2005.

14. Medlock, K. L. Gates and Longuski, J. M., "An Approach to Sizing a Dual-Use Ballute System for Aerocapture, Descent and Landing," 4th International Planetary Probe Workshop, Pasadena, CA, June 27–30, 2006.

15. Gates, K. L., McRonald, A. D., and Nock, K. T., "HyperPASS, a New Aeroassist Tool," 2nd International Planetary Probe Workshop, NASA Ames Research Center, Moffet Field, CA, Aug. 2004.

16. Bird, G. A., Molecular Gas Dynamics and the Direct Simulation of Gas Flows, Clarendon Press, Oxford, 1994.

17. Ivanov, M. S., Markelov, G. N., and Gimelshein, S. F., "Statistical Simulation of Reactive Flows: Numerical Approach and Applications", AIAA Paper 1998-2669.

18. Moss, J., "DSMC Simulations of Ballute Aerothermodynamics Under Hypersonic Rarefied Conditions," 38th AIAA Thermophysics Conference, Toronto, Ontario Canada, June 2005.

19. Gnoffo, P., Buck, G., Moss, J., Nielsen, E., Berger, K., Jones, W. T., and Rudavsky, R., "Aerothermodynamic Analyses of Towed Ballutes," 9th AIAA/ASME Joint Thermophysics and Heat Transfer Conference, San Francisco, CA, June 2006.

20. Sutton, K. and Graves, R. A., Jr., "A General Stagnation Point Convective Heating Equation for Arbitrary Gas Mixtures," NASA TR R-376, NASA Langley Research Center, Hampton, VA, Nov. 1971.

21. Hash, D. B. and Hassan, H. A., "Monte Carlo Simulation of Entry in the Martian Atmosphere", *Journal of Thermophysics and Heat Transfer*, Vol. 7, No. 2, pp. 228-232, 1993.

22. Borgnakke, C., and Larson, P. S., “Statistical Collision Model for Monte Carlo Simulation of Polyatomic Gas Mixture,” *Journal of Computational Physics*, Vol. 18, Mo. 4, 1975, pp. 405–420.

23. Alexeenko, A. A., *Gas Dynamics Toolbox*, JAVA applet, http://web.ics.purdue.edu /~alexeenk/GDT/index.html.

24. Pitts, D. E., et al., "The Mars Atmosphere: Observations and Model Profiles for Mars Missions," NASA Johnson Space Center report JSC-24455, 1990.